Journal of Energy Chemistry 25 (2016) 1038–1044

Contents lists available at ScienceDirect

Journal of Energy Chemistry

journal homepage: www.elsevier.com/locate/jechem

http://www.journals.elsevier.com/journal-of-energy-chemistry/

Synergistic effects of bimetallic Cu-Fe/SiO_2 nanocatalysts in selective hydrogenation of diethyl malonate to 1,3-propanediol

Le He, Xiaoxiao Gong, Linmin Ye*, Xinping Duan, Youzhu Yuan*

State Key Laboratory of Physical Chemistry of Solid Surfaces, National Engineering Laboratory for Green Chemical Production of Alcohols-Ethers-Esters, Collaborative Innovation Center of Chemistry for Energy Materials, College of Chemistry and Chemical Engineering, Xiamen University, Xiamen 361005, Fujian, China

ARTICLE INFO

Article history:
Received 26 July 2016
Revised 23 September 2016
Accepted 16 October 2016
Available online 15 November 2016

Keywords:
Bimetallic catalyst
Hydrogenation
1,3-Propanediol
Cu–Fe
Synergistic effect

ABSTRACT

Cu_x–Fe_y/SiO_2 catalysts were prepared using urea-assisted sol–gel method. The structure and physicochemical properties of the catalysts were characterized using N_2 adsorption–desorption, transmission electron microscopy, H_2-temperature-programmed reduction, powder X-ray diffraction, and X-ray photoelectron spectroscopy. Compared with monometallic Cu or Fe catalysts, the bimetallic Cu_x–Fe_y/SiO_2 catalysts exhibited enhanced catalytic performance for the selective hydrogenation of diethyl malonate to 1,3-propanediol. The bimetallic catalyst with an optimal Cu/Fe atomic ratio of 2 exhibited the highest activity, which yielded 96.3% conversion to diethyl malonate and 93.3% selectivity to 1,3-propanediol under the optimal reaction conditions. Characterization results revealed that interactions between Cu and Fe contributed to the improvement of diethyl malonate conversion and selectivity to 1,3-propanediol. The X-ray photoelectron spectroscopy results revealed that the addition of appropriate amount of Fe species enhanced the reduction of Cu^{2+} species, thereby increasing the Cu^0 species on the surface of bimetallic catalyst. It led to a better chemisorption capacity of hydrogen and further promoted of the activation of hydrogen molecule. The ethyl acetate temperature-programmed desorption results indicated that the FeO_x species provided the additional adsorption sites for substrate molecules, and they activated the C=O bond. The improved catalytic performance of bimetallic Cu_x–Fe_y/SiO_2 catalyst was mainly attributed to the synergistic effect between Cu^0 and FeO_x species.

1. Introduction

1,3-Propanediol (1,3-PDO) is an important building block in polyester industry, which is used for the production of functional polyester material named as poly-1,3-trimethylene terephthalate (PTT). This material exhibits a number of advantages over traditional polyesters based on ethylene glycol or 1,4-butanediol and terephthalic acid [1]. For example, PTT shows excellent stretch recovery characteristic, which is mainly caused by the different molecular structures. However, the limited production of 1,3-PDO restricts the development of PTT material. The two major petrochemical routes for the industrial production of 1,3-PDO are the hydroformylation of ethylene oxide [2,3] and hydration of acrolein [4]. The intermediates of these two methods are unstable, thereby leading to a low selectivity to 1,3-PDO. In addition, other several methods, such as hydrogenolysis of glycerol [5,6], bioconversion of glycerol [7,8], and functionalization of primary C–H bond of *n*-propanol [9], are still at the laboratory scale. Therefore, hydrogenation of syngas-based or biomass-based diethyl malonate (DEM) to produce 1,3-PDO is a promising route that combines the energy structure features of China.

Copper-based catalysts show excellent activity in the hydrogenation of various esters to corresponding alcohols [10–12]. In the hydrogenation of dimethyl oxalate (DMO), copper-based catalysts are effective for the production of ethylene glycol [13] and ethanol [14]. According to the primary mechanism of Cu-catalyzed DMO hydrogenation proposed in the literature, Cu^0 and Cu^+ species are present in the reaction for hydrogen dissociation and activation of C=O bond, respectively [15,16]. The synergistic effect of these two Cu species makes the catalyst effective. Nevertheless, copper-based catalyst easily deactivates during the reaction process, which is mainly caused by the imbalance of active species, Ostwald ripening induced by CO, and aggregation of Cu nanoparticles [17,18]. In the prior literature of our group, two methods are used for the improvement of activity and stability, one is introduction of different additives, such as La [19], B [20], and HZSM-5 [21], the other is to form alloys, such as Ag–Cu [22], Au–Cu [23], and Pt–Cu [24]. Unlike DMO, the hydrogenation of DEM is a complicated process. Ethyl 3-hydroxypropanoate (3-HPE), as the

* Corresponding author. Fax: +86 592 2183047.
E-mail addresses: lmye@xmu.edu.cn (L. Ye), yzyuan@xmu.edu.cn (Y. Yuan).

http://dx.doi.org/10.1016/j.jechem.2016.11.007

primary product, is easily dehydrated to form a stable conjugate structure that increases the selectivity to *n*-propanol. Adkins et al. [25] first reported that 1,3-PDO could be produced via catalytic hydrogenation of malonate with Cu–Cr catalyst under high pressure. However, less than 40% yield of 1,3-PDO is not satisfactory. Moreover, Cr is toxic and harmful to the environment. Recently, Ding et al. [26] reported that boron promotes Cu/SiO_2 catalyst prepared via ammonia evaporation co-precipitation method for the hydrogenation of DEM to 1,3-PDO with a selectivity of 30%. Boron, as a promoter, could increase the formation of Cu^0 species, which enhances selectivity. Supported Au–Ag bimetallic catalysts can be used for the gas-phase selective hydrogenation of dimethyl malonate to methyl 3-hydroxypropanoate with a selectivity of 81.6% [27]. With the higher hydrogenation ability of Cu than Ag or Au, a bimetallic Cu-based catalyst may be considered for the hydrogenation of DEM to 1,3-PDO.

In the current study, we reported a series of bimetallic Cu_x–Fe_y/SiO_2 catalysts synthesized through urea-assisted sol–gel method and used for the hydrogenation of DEM to 1,3-PDO. The Cu_x–Fe_y/SiO_2 catalyst displayed excellent catalytic performance in the selective hydrogenation of DEM to 1,3-PDO under the optimal reaction conditions. The structures of Cu and Fe were characterized using powder X-ray diffraction (XRD), transmission electron microscopy (TEM), and X-ray photoelectron spectroscopy (XPS). The function of Fe species was demonstrated by utilizing the ethyl acetate temperature-programmed desorption (TPD) result. The relationship between the structure and catalytic performance of the catalyst was also addressed.

2. Experimental

2.1. Catalyst preparation

The bimetallic Cu_x–Fe_y/SiO_2 catalysts with a preset Cu loading amount of 10 wt% were synthesized through urea-assisted sol–gel method, which is similar to our prior literature [20,21]. Briefly, quantitative amount of 40 wt% Ludox AS-40 colloidal silica was dispersed in 100 mL of aqueous solution containing 5.0 g of urea and desired amount of $Cu(NO_3)_2\cdot 3H_2O$ and $Fe(NO_3)_3\cdot 9H_2O$ in a round-bottomed flask. The suspension was vigorously stirred at 363 K for 8 h. The obtained precipitate was separated via hot filtration and washed for three times with deionized water. The obtained powder was dried at 383 K overnight and calcined in air at 623 K for 4 h. Before catalytic evaluation, the precursors were reduced at 623 K at a temperature ramping rate of 2 K/min using 5% H_2−95% N_2 gas for 4 h. The catalyst was labeled as Cu_x–Fe_y/SiO_2, where x and y are the atomic ratios of Cu and Fe, respectively. The monometallic catalysts, Cu/SiO_2 and Fe/SiO_2, were also prepared following that similar synthesis procedure. For comparison, the control catalyst prepared through post-impregnation method using Cu/SiO_2 as precursor was denoted as Cu_x–Fe_y/SiO_2-IM.

2.2. Catalyst characterization

The actual contents of Cu and Fe elements were determined through X-ray fluorescence spectrometry (XRF) using a Bruker S8 TIGER spectrometer. XRD analysis was performed with a PANalytical X'pert Pro Super X-ray diffractometer using Cu K_α radiation ($\lambda = 0.15418$ nm) with scanning angle (2θ) ranging from 10° to 90°. The XRD pattern was identified through matching the results with reference patterns that were included in the JCPDS database. TEM images were obtained on a Tecnai F30 apparatus operated at 300 kV. Elemental distribution in the catalysts was determined through energy-dispersive X-ray spectroscopy (EDX) at scanning TEM (STEM) mode. The statistical mean diameter of the nanoparticles was measured through counting at least 200 particles for each catalyst. Nitrogen adsorption–desorption isotherms were measured using static N_2 physisorption at 77.3 K with a Micromeritics TriStar II 3020 surface area and pore analyzer. The surface area and mesopore diameter were calculated according to the BET and BJH methods, respectively. Hydrogen temperature-programmed reduction (H_2-TPR) for the as-calcined catalyst samples and the TPD for ethyl acetate absorbed on the as-reduced samples were measured on a Micromeritics Autochem II 2920 instrument connected to a Hiden Qic-20 mass spectrometer [28]. The copper dispersion of the catalysts was determined on a Micromeritics Autochem II 2920 apparatus with a thermal conductivity detector (TCD) through N_2O chemisorption and H_2 pulse reduction methods based on the stoichiometry of $[2Cu(s)+N_2O\rightarrow Cu_2O(s)+N_2]$, where Cu(s) represents the surface copper atom [29]. XPS was performed using a PHI QUANTUM 2000 Scanning ESCA Microprobe instrument with an Al-K_α radiation source ($h\nu = 1486.6$ eV). The binding energy was calibrated from that of C 1*s* (284.6 eV). Prior to measurements, each sample was pressed into a thin disk and pretreated in an atmosphere of 5% H_2-95% N_2 at 693 K for 3 h.

2.3. Catalytic test

The hydrogenation of DEM was carried out in a fixed-bed reactor equipped with a computer-controlled auto-sampling system. Typically, 100 mg of catalyst (40–60 mesh) was loaded into the center of the reactor, and both sides of the catalyst were packed with quartz powders (40–60 mesh) to minimize the dead volume. 5 wt% DEM–ethanol mixed solution with a preset flow rate of 0.02 mL/min (LHSV = 0.6 h^{-1}) was pumped into the system with a Series III digital HPLC pump (Scientific Systems, Inc.). The reaction temperature was 483 K with H_2/DEM molar ratio of 350 (the H_2 flow rate was 53.5 mL/min). The products were analyzed through an online gas chromatograph (GC, FuLi 9790-II) equipped with a flame ionization detector and a capillary column (KB-Wax, 60 m × 0.32 mm × 0.33 μm), as well as another GC equipped with a TCD detector and a packed column (Gaskuropack 54, 3 m). The conversion and product selectivities were calculated by using the calibrated normalization method.

The TOF value was calculated by the following formula while the conversion was controlled below 40%.

$$\mathrm{TOF} = \frac{V \times C_{\mathrm{DEM}} \times X_{\mathrm{DEM}}}{D \times N_{\mathrm{M}}}$$

where, V represents the flow rate of DEM solution (L/h), C_{DEM} is the concentrate of DEM (mol/L), X_{DEM} is the conversion of DEM, D is the metal dispersion of Cu particles, N_{M} is the mole of Cu loading amount.

3. Results and discussion

3.1. Physicochemical characterization

The physicochemical properties of bimetallic Cu_x–Fe_y/SiO_2 catalysts are illustrated in Table 1. The XRF results demonstrated that the Cu content was maintained at about 10 wt%. With the increase of Fe content, the BET surface area and pore volume gradually decreased. The BET surface area of monometallic Cu/SiO_2 was 251.7 m^2/g, which was twice than that of Fe/SiO_2; such area mainly resulted from the formation of copper phyllosilicate species. In addition, the BET surface area of Cu_2–Fe_1/SiO_2-IM sample prepared via post-impregnation method was smaller than that of Cu_2–Fe_1/SiO_2, thereby indicating that urea-assisted sol–gel method was the appropriate method for catalyst preparation. Fig. 1 shows the XRD patterns of as-reduced samples with different Cu/Fe atomic ratios. The broad and weak diffraction lines of Cu(111) were observed at 43.2° (JCPDS = 004-0836), which suggested a well dispersion of Cu species on SiO_2. For the monometallic Fe/SiO_2, the

Table 1. Physicochemical properties of Cu_x–Fe_y/SiO_2 catalysts.

Sample	Cu[a] (wt%)	Fe[a] (wt%)	S_{BET} (m^2/g)	V_{pore}[b] (cm^3/g)	$D_{particle}$[c] (nm)	D_{Cu}[d] (%)
Cu/SiO_2	10.4		251.7	0.66	5.2	29.2
Cu_{10}–Fe_1/SiO_2	9.6	0.8	183.3	0.52	4.6	31.5
Cu_5–Fe_1/SiO_2	9.9	1.4	172.6	0.51	4.9	32.3
Cu_2–Fe_1/SiO_2	10.1	3.2	167.2	0.50	4.5	29.3
Cu_1–Fe_1/SiO_2	9.5	4.7	158.3	0.51	5.2	30.4
Cu_1–Fe_2/SiO_2	9.8	6.5	152.3	0.50	5.2	28.7
Fe/SiO_2	–	11.3	108.1	0.47	–	–
Cu_2–Fe_1/SiO_2–IM	9.8	3.1	145.4	0.43	4.7	29.1

[a] Determined by XRF analysis.
[b] Obtained from $P/P_0 = 0.99$.
[c] The particle size was estimated from the TEM images.
[d] Cu dispersion determined by N_2O chemisorption and H_2 pulse reduction.

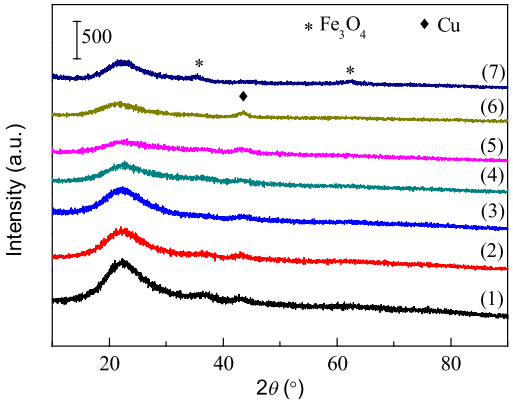

Fig. 1. XRD patterns of as-reduced catalysts: (1) Cu/SiO_2, (2) Cu_{10}–Fe_1/SiO_2, (3) Cu_5–Fe_1/SiO_2, (4) Cu_2–Fe_1/SiO_2, (5) Cu_1–Fe_1/SiO_2, (6) Cu_1–Fe_2/SiO_2, (7) Fe/SiO_2.

diffraction lines of Fe_3O_4 were observed at $2\theta = 35.8°$ and 64.2° (JCPDS = 002-1035). Fe_2O_3 can only be reduced to Fe_3O_4 under current reduction conditions [30]. Cu–Fe alloy showed no diffraction lines according to the XRD. The metal particle size of catalysts was estimated from the TEM images via measuring more than 200 particles (Fig. 2). The average particle size of monometallic Cu/SiO_2 was 5.2 nm. With the addition of Fe species, the particle size of bimetallic Cu_x–Fe_y/SiO_2 decreased slightly and was maintained at about 5 nm. The Cu_2–Fe_1/SiO_2 sample displayed the smallest Cu nanoparticle size of 4.5 nm, which indicated that the introduction of proper amount Fe species was beneficial to Cu dispersion. This observation was also verified by the Cu dispersion results.

Fig. 3 displays the H_2-TPR profiles of Cu_x–Fe_y/SiO_2 catalysts. The monometallic Cu/SiO_2 showed a reduction peak at about 532 K. The monometallic Fe/SiO_2 displayed a weak and broad reduction peak ranging from 550 to 750 K, which is mainly caused by the overlap of the two reduction peaks of Fe^{3+} to Fe^{2+} and Fe^{2+} to Fe [31]. With the increase of Fe species, the reduction peak moves to a lower temperature. Furthermore, a shoulder peak arises at 460 K, which is attributed to the reduction of highly dispersed CuO species [32,33]. The H_2-TPR profile results suggested that some interactions between Cu and Fe occurred, and the introduction of Fe species accelerated the reduction of Cu^{2+} species to metallic Cu.

3.2. Catalytic performance

The major products in the hydrogenation of DEM were 3-HPE, 1,3-PDO, *n*-propanol, ethyl propionate, ethyl acetate, and less than 1% gas phase products, which were mainly CO_2 and CH_4.

Table 2. Catalytic performance of Cu_x–Fe_y/SiO_2 catalysts with different Cu/Fe atomic ratios[a].

Catalyst	Conversion (%)	Selectivity (%)				TOF[c] (h^{-1})
		1,3-PDO	3-HPE	*n*-propanol	Others[b]	
Cu/SiO_2	85.4	78.5	12.3	4.2	5.0	8.3
Cu_{10}–Fe_1/SiO_2	88.7	83.9	3.8	5.2	7.1	14.1
Cu_5–Fe_1/SiO_2	93.3	86.3	2.6	3.2	7.9	14.9
Cu_2–Fe_1/SiO_2	96.3	93.3	2.5	1.2	3.0	17.3
Cu_1–Fe_1/SiO_2	72.7	76.7	18.2	1.1	4.0	13.0
Cu_1–Fe_2/SiO_2	54.1	68.0	26.5	0.8	4.7	6.8
Fe/SiO_2	0	0	0	0	0	0
Cu_2–Fe_1/SiO_2–IM	86.5	71.3	15.5	3.6	9.6	8.6

[a] Reaction conditions: $P = 5.0$ MPa, $T = 483$ K, H_2/DEM = 350 (molar ratio), LHSV = 0.6 h^{-1}. The data were obtained after the reaction proceeded for 5 h when the steady state was reached.
[b] Mainly containing ethyl propionate and ethyl acetate.
[c] The TOF was calculated by Cu dispersion when the conversion was controlled under 40%.

Table 3. Deconvolution results of Cu LMM XAES for Cu_x–Fe_y/SiO_2 catalysts.

Catalyst	Kinetic energy (eV)		Auger parameter (eV)		Cu $2p_{3/2}E_b$ (eV)	X_{Cu0}[a] (%)
	Cu^+	Cu^0	Cu^+	Cu^0		
Cu/SiO_2	913.3	917.1	1846.1	1849.9	932.8	49.3
Cu_{10}–Fe_1/SiO_2	913.6	917.6	1846.4	1850.4	932.8	51.5
Cu_5–Fe_1/SiO_2	913.2	917.4	1846.0	1850.2	932.8	53.4
Cu_2–Fe_1/SiO_2	913.7	917.4	1846.5	1850.2	932.8	53.9
Cu_1–Fe_1/SiO_2	913.3	917.1	1846.1	1849.9	932.8	53.7
Cu_1–Fe_2/SiO_2	913.5	917.5	1846.3	1850.3	932.8	54.5

[a] Intensity ratio between Cu^0 and ($Cu^0 + Cu^+$) by deconvolution of Cu LMM XAES spectra.

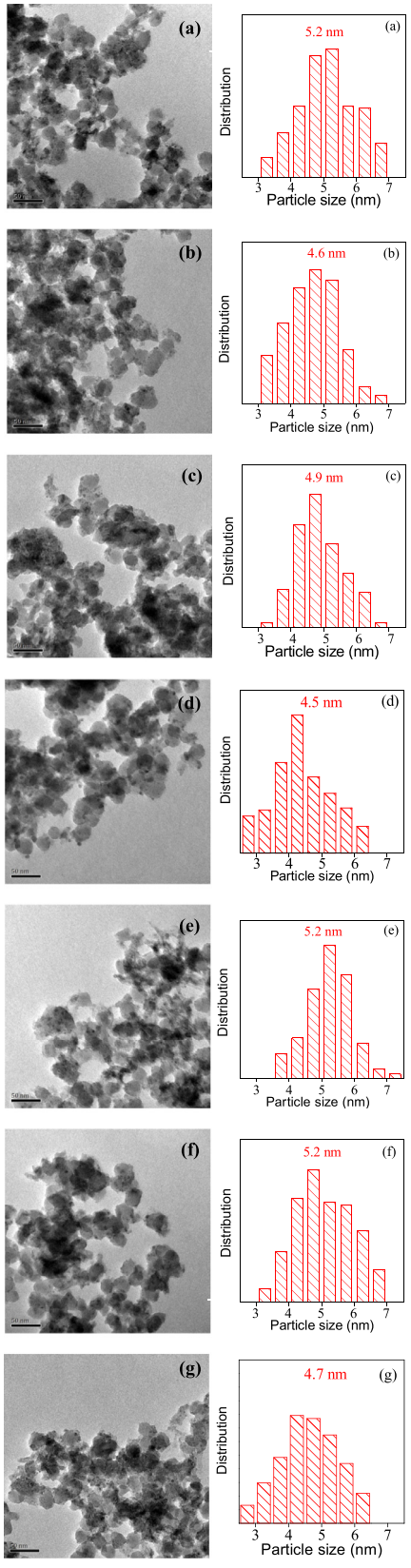

Fig. 2. TEM images and metal particle size distributions of as-reduced catalysts: (a) Cu/SiO_2, (b) $Cu_{10}–Fe_1/SiO_2$, (c) $Cu_5–Fe_1/SiO_2$, (d) $Cu_2–Fe_1/SiO_2$, (e) $Cu_1–Fe_1/SiO_2$, (f) $Cu_1–Fe_2/SiO_2$, (g) $Cu_2–Fe_1/SiO_2$-IM.

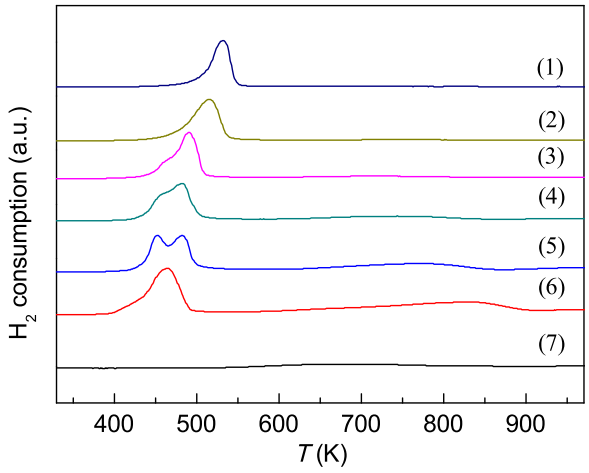

Fig. 3. H_2-TPR profiles of as-calcined catalysts: (1) Cu/SiO_2, (2) $Cu_{10}–Fe_1/SiO_2$, (3) $Cu_5–Fe_1/SiO_2$, (4) $Cu_2–Fe_1/SiO_2$, (5) $Cu_1–Fe_1/SiO_2$, (6) $Cu_1–Fe_2/SiO_2$, (7) Fe/SiO_2.

Therefore, the selectivity to gas phase products was not calculated in this research. First, Cu/SiO_2 catalyst was used to evaluate the optimal reaction conditions for the hydrogenation of DEM to 1,3-PDO. The reaction parameters, such as reaction temperature, hydrogen pressure, and H_2/DEM molar ratio, influenced the catalytic performances remarkably. The conversion of DEM increased when the reaction temperature increased from 473 to 493 K (Fig. 4a). Selectivity to 1,3-PDO showed a volcano-type curve and peaked at 483 K with a selectivity to 1,3-PDO of 78.5%. Further increase of the reaction temperature led to a high selectivity to *n*-propanol, which was one of the over-hydrogenation byproducts. The influence of hydrogen pressure and H_2/DEM molar ratio is shown in Fig. 4(b) and (c), respectively. The changes in conversion and selectivity were similar to the reaction temperature. The increase of hydrogen pressure and H_2/DEM molar ratio improved the active H species in the reaction. Unlike DMO, no conjugated structure was observed in the DEM molecule. Therefore, high hydrogen pressure and H_2/DEM molar ratio were needed for the activation of this inactive diester. The optimal reaction conditions were hydrogen pressure of 5.0 MPa, reaction temperature of 483 K, and H_2/DEM molar ratio of 350.

The catalytic performance of $Cu_x–Fe_y/SiO_2$ catalysts with different Cu/Fe atomic ratios was evaluated under the optimal reaction conditions (Table 2). Fe/SiO_2 showed little activity, which confirmed that Fe species alone has no effect on the hydrogenation of DEM. This result also implied that the active metal Cu played a vital role in the hydrogenation of DEM. However, both the conversion and selectivity to 1,3-PDO increased with the introduction of proper amount of Fe species. The optimal Cu/Fe ratio was 2. The conversion and selectivity to 1,3-PDO reached 96.3% and 93.3%, respectively. Further increase of Fe species rapidly decreased the conversion and selectivity, which was mainly caused by the excess FeO_x species covering the active Cu surface. The turnover frequency (TOF) was calculated when the conversion was controlled under 40%. The highest TOF value of 17.3 h^{-1} was obtained using the $Cu_2–Fe_1/SiO_2$ catalyst. The preparation method was also considered. $Cu_2–Fe_1/SiO_2$-IM catalyst showed similar catalytic performance to that of monometallic Cu/SiO_2, which indicated that interaction between Cu and Fe species is important in the hydrogenation of DEM to 1,3-PDO.

3.3. Effect of Fe species

TEM, XPS, and TPD measurements were used for further investigation of the interaction between Cu and Fe species to reveal the effect of Fe species of bimetallic $Cu_x–Fe_y/SiO_2$ catalyst. As

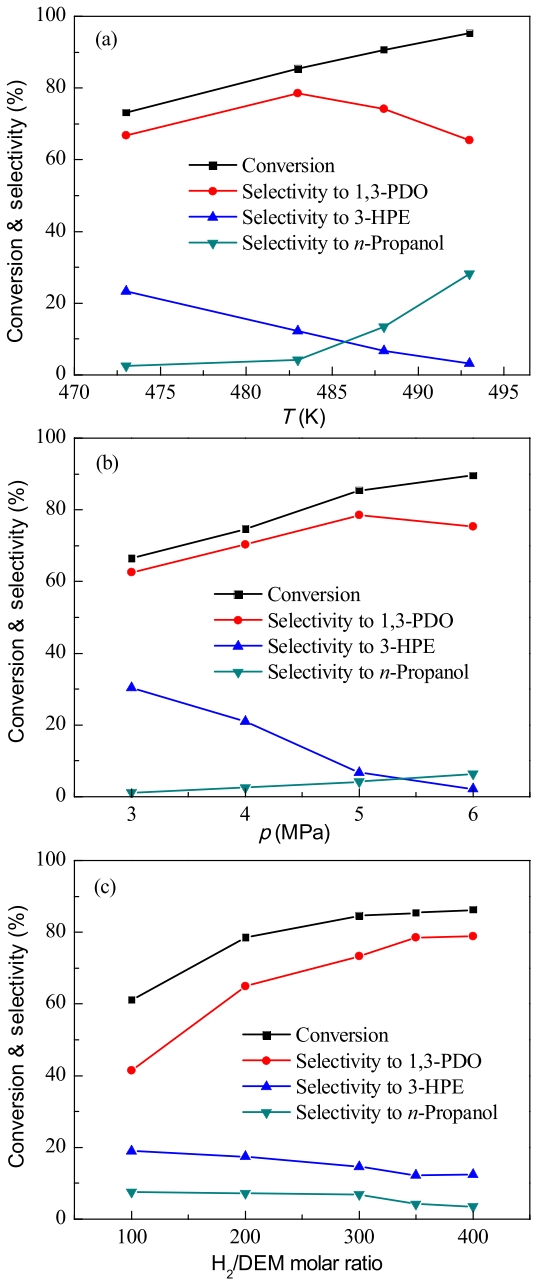

Fig. 4. Influence of reaction parameters on the hydrogenation of DEM over Cu/SiO_2: (a) T, (b) p, (c) H_2/DEM molar ratio. Reaction conditions: $T = 483$ K, $P = 5.0$ MPa, H_2/DEM = 350 (molar ratio), LHSV = 0.6 h^{-1}. The data were obtained after the reaction proceeded for 5 h when the steady state was reached.

shown in Fig. 5, the structure of catalyst was further characterized via high-resolution TEM (HR-TEM). Well-resolved lattice fringe was clearly observed, and only one lattice fringe with interplanar spacing of 0.2080 nm appeared, which was ascribed to the (111) plane of metallic Cu (JCPDS = 004-0836). There is no Cu–Fe alloy formed in both catalysts prepared by different method. It is reported that the Cu and Fe are difficult to form the alloy phase while the reduction temperature was lower than 800 K [34,35]. The HAADF-STEM and EDX elemental mapping in STEM mode were also adopted to investigate the distribution of Cu and Fe atoms of the catalyst. The elemental EDX maps showed the Cu and Fe species were well dispersed in Cu_2–Fe_1/SiO_2 catalyst. Therefore, they can interact with each other. The close integration of Cu and Fe species may be the origin of the synergistic effect. In contrast, the agglomeration of Fe species was observed in Cu_2–Fe_1/SiO_2-IM prepared by post-impregnation method, leading to a weaker interaction between Cu and Fe species. It may be responsible for the different catalytic performances in Table 2.

The Cu LMM XAES data provided the information regarding the Cu species on the surface of Cu_x–Fe_y/SiO_2 catalysts. Two kinds of Cu species could be identified (Fig. 6). The kinetic energy of 913.4 and 917.5 eV are attributed to Cu^+ and Cu^0, respectively [19–24]. The fitting results are summarized in Table 3, and the ratio of Cu^0 was calculated according to the following formula: $Cu^0/(Cu^0 + Cu^+)$. The monometallic Cu/SiO_2 showed a Cu^0 ratio of 49.3%. The existence of Cu^0 species was assumed to play an important role in the activation of hydrogen molecule. The proportion of surface Cu^0 species on the bimetallic Cu_x–Fe_y/SiO_2 catalysts improved to about 54% with the increase of Fe. Therefore, the Fe species was beneficial for the reduction of Cu^{2+} to Cu^0, which was consistent with the H_2-TPR results.

The XRD and TEM results indicated that the Fe species could hardly be reduced to metallic Fe under current reduction condition. Thus, the function of FeO_x species in the reaction should be determined. There are two active sites in this reaction: the Cu^0 is for the activation of hydrogen; and the Cu^+ and FeO_x are for the adsorption of substrate. Due to the high boiling point, the ethyl acetate was introduced instead of DEM for the TPD measurement. The ethyl acetate TPD result can provide the information of adsorption sites. Fig. 7 shows two major desorption peaks at 350 and 600 K, which were attributed to the physical and chemical adsorption of ethyl acetate, respectively. Compared with Cu/SiO_2, Fe/SiO_2 exhibited stronger adsorption ability of C=O bond. Therefore, the addition of Fe species in the Cu/SiO_2 enhanced the interaction between catalyst and ester, and activated the C=O bond in the hydrogenation reaction. The synergistic effect of Cu^0 and FeO_x species in bimetallic Cu_2–Fe_1/SiO_2 catalyst may have caused the higher catalytic performance than that of monometallic Cu/SiO_2.

As reported by Ding et al., the hydrogenation of DEM is a multi-step reaction including the hydrogenation of DEM to 3-HPE as an intermediate, hydrogenation of 3-HPE to 1,3-PDO, and over-hydrogenation of 1,3-PDO to *n*-propanol [36]. In this work, the major products are 1,3-PDO and 3-HPE. The proposed mechanism of synergistic effect in the hydrogenation of DEM over bimetallic Cu–Fe/SiO_2 bimetallic catalyst was showed in Scheme 1. The Cu^0 is for the activation of hydrogen molecule. The Fe species has two functions in this reaction: one is promoting the reduction of Cu^{2+} or Cu^+ to form more Cu^0 species, which increased the conversion of DEM simultaneously; the other is providing extra active site for the adsorption of oxygen-containing substrates, such as DEM and 3-HPE. The synergistic effect of Cu^0 and FeO_x species accelerates the hydrogenation DEM to 1,3-PDO.

3.4. Catalyst stability

The long-term performance of Cu_2–Fe_1/SiO_2 was evaluated in order to investigate the stability of bimetallic catalyst. As shown in Fig. 8, the optimal Cu–Fe/SiO_2 bimetallic catalyst with Cu/Fe ratio of 2 kept 85% selectivity to 1,3-PDO till 50 h time on steam. However, the conversion and selectivity dropped to less than 80% suddenly when prolonging the reaction time. The selectivity to 1,3-PDO decreased while the selectivity to 3-HPE increased, indicating the decreasing of hydrogenation ability of Cu–Fe/SiO_2 bimetallic catalyst. The XRD result demonstrated the Cu nanoparticle sintered during the reaction process. Ding et al. reported a similar phenomenon in this reaction [36]. Therefore, the aggregation of Cu nanoparticle may be responsible for the deactivation of Cu–Fe/SiO_2 bimetallic catalyst.

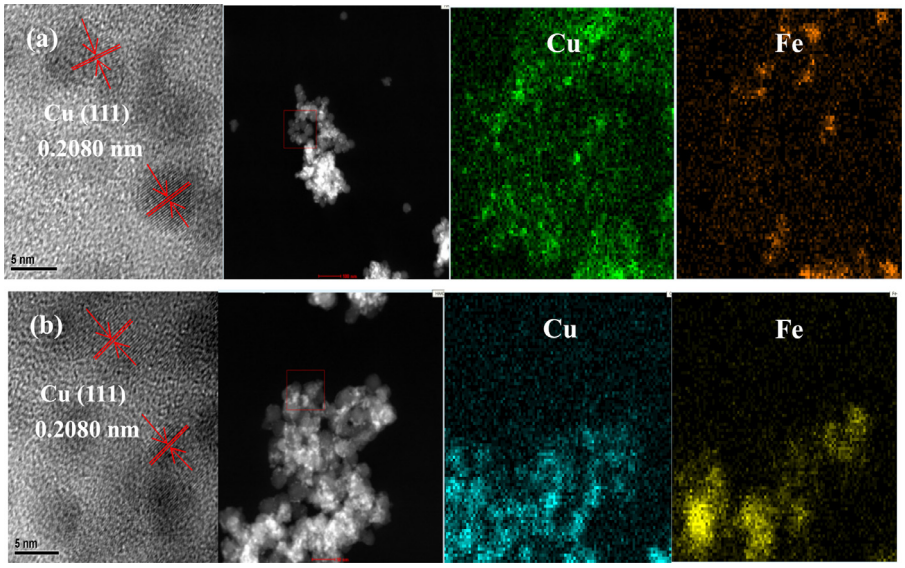

Fig. 5. HR-TEM, HAADF-STEM images and elemental EDX maps of reduced catalysts: (a) Cu_2–Fe_1/SiO_2 and (b) Cu_2–Fe_1/SiO_2–IM.

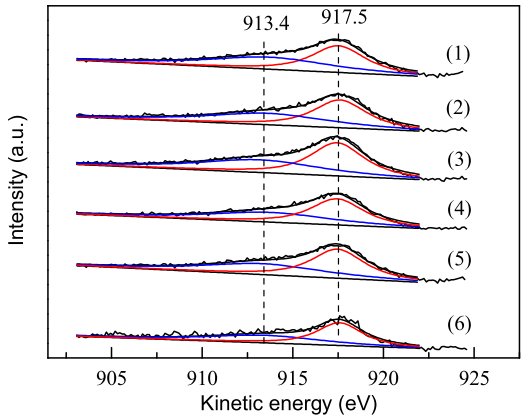

Fig. 6. Cu LMM XAES spectra of catalysts. (1) Cu/SiO_2, (2) Cu_{10}–Fe_1/SiO_2, (3) Cu_5–Fe_1/SiO_2, (4) Cu_2–Fe_1/SiO_2, (5) Cu_1–Fe_1/SiO_2, (6) Cu_1–Fe_2/SiO_2.

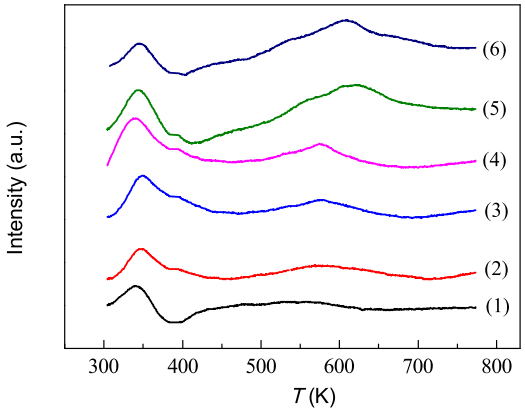

Fig. 7. Ethyl acetate TPD profiles of catalysts. (1) Cu/SiO_2, (2) Cu_{10}–Fe_1/SiO_2, (3) Cu_5–Fe_1/SiO_2, (4) Cu_2–Fe_1/SiO_2, (5) Cu_1–Fe_2/SiO_2, (6) Fe/SiO_2.

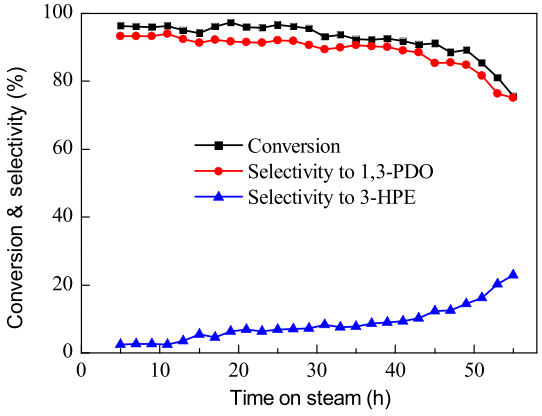

Fig. 8. Long-term performance of DEM hydrogenation over Cu_2–Fe_1/SiO_2 catalyst. Reaction conditions: $T = 483$ K, $P = 5.0$ MPa, H_2/DEM = 350 (molar ratio), LHSV = 0.6 h^{-1}.

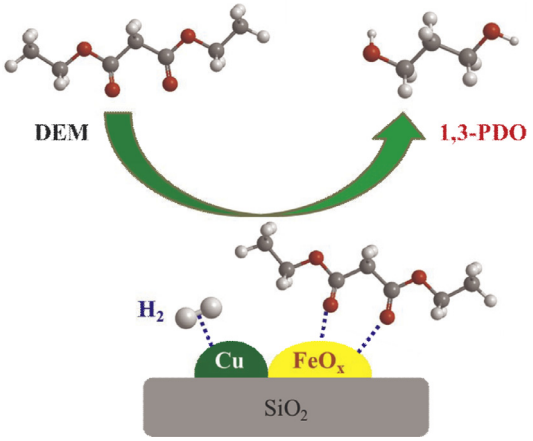

Scheme 1. Proposed mechanism of synergistic effect in the hydrogenation of DEM over Cu–Fe/SiO_2 bimetallic catalyst.

4. Conclusions

Cu_2–Fe_1/SiO_2 bimetallic catalyst prepared via urea-assisted sol–gel method showed excellent catalytic performance on the hydrogenation of DEM to 1,3-PDO. The conversion and selectivity to 1,3-PDO reached 96.3% and 93.3% under optimal reaction conditions, respectively. To the best of our knowledge, the obtained value was the highest selectivity reported on the hydrogenation

of DEM to 1,3-PDO. XRD and TEM demonstrated that Cu and Fe didn't form the alloy phase. Further evidence obtained from XPS and TPD measurement indicated that the addition of Fe species was beneficial for the reduction of Cu^{2+} to Cu^0, and it provided additional adsorption site for the ester substrate. The synergistic effect of Cu^0 and FeO_x species in bimetallic Cu_2–Fe_1/SiO_2 catalyst may be the reason for the higher catalytic performance than that of monometallic Cu/SiO_2 in the hydrogenation of DEM to 1,3-PDO.

Acknowledgments

This work was supported by the Natural Science Foundation of China (91545115, 21473145, and 21403178), the Postgraduate Basic Innovative Research Program of Xiamen University (201412G001), and the Program for Innovative Research Team in Chinese Universities (no. IRT_14R31).

References

[1] G.A. Kraus, Clean 36 (2008) 648–651.
[2] P.R. Weider, J.B. Powell, K.T. Lam, US5684214A, 1997.
[3] J.B. Powell, S.B. Mullin, P.R. Weider, D.C. Eubanks, J.P. Arhancet, US5770776A, 1998.
[4] D. Arntz, N. Wiegand, EP412337A2, 1991.
[5] D.L. Sun, Y. Yamada, S. Sato, W. Ueda, Appl. Catal. B Environ. 193 (2016) 75–92.
[6] Y.L. Wang, J.X. Zhou, X.W. Guo, RSC Adv. 5 (2015) 74611–74628.
[7] C.S. Lee, M.K. Aroua, W.M.A.W. Daud, P. Cognet, Y. Pérès-Lucchese, P-L. Fabre, O. Reynes, L. Latapie, Renew. Sust. Energ. Rev. 42 (2015) 963–972.
[8] G. Kaur, A.K. Srivastava, S. Chand, Biochem. Eng. J. 64 (2012) 106–118.
[9] E.M. Simmons, J.F. Hartwig, Nature 483 (2012) 70–73.
[10] T. Turek, D.L. Trimm, Catal. Rev. Sci. Eng. 36 (1994) 645–683.
[11] Z.P. Lu, H.B. Yin, A.L. Wang, J. Hu, W.P. Xue, H.X. Yin, S.X. Liu, J. Ind. Eng. Chem. 37 (2016) 208–215.
[12] Y.Q. Yang, X.L. Xu, W.J. Zou, H.J. Yue, G. Tian, S.H. Feng, Catal. Commun. 76 (2016) 50–53.
[13] H.R. Yue, Y.J. Zhao, X.B. Ma, J.L. Gong, Chem. Soc. Rev. 41 (2012) 4218–4244.
[14] H.R. Yue, X.B. Ma, J.L. Gong, Acc. Chem. Res. 47 (2014) 1483–1492.
[15] L.F. Chen, P.J. Guo, M.H. Qiao, S.R. Yan, H.X. Li, W. Shen, H.L. Xu, K.N. Fan, J. Catal. 257 (2008) 172–180.
[16] A.Y. Yin, X.Y. Guo, W.L. Dai, K.N. Fan, J. Phys. Chem. C 113 (2009) 11003–11013.
[17] R.H. Ouyang, J.X. Liu, W.X. Li, J. Am. Chem. Soc. 135 (2013) 1760–1771.
[18] J.W. Zheng, J.F. Zhou, H.Q. Lin, X.P. Duan, C.T. Williams, Y.Z. Yuan, J. Phys. Chem. C 119 (2015) 13758–13766.
[19] X.L. Zheng, H.Q. Lin, J.W. Zheng, X.P. Duan, Y.Z. Yuan, ACS Catal. 49 (2013) 2451–2453.
[20] Z. He, H.Q. Lin, P. He, Y.Z. Yuan, J. Catal. 277 (2011) 54–63.
[21] H.Q. Lin, X.L. Zheng, Z. He, J.W. Zheng, X.P. Duan, Y.Z. Yuan, Appl. Catal. A Gen. 445 (2012) 287–296.
[22] Y. Huang, H. Ariga, X.L. Zheng, X.P. Duan, S. Takakusagi, K. Asakura, Y.Z. Yuan, J. Catal. 307 (2013) 74–83.
[23] Y.N. Wang, X.P. Duan, J.W. Zheng, H.Q. Lin, Y.Z. Yuan, H. Ariga, S. Takakusagi, K. Asakura, Catal. Sci. Technol. 2 (2012) 1637–1639.
[24] X.L. Zheng, H.Q. Lin, J.W. Zheng, H. Ariga, K. Asakura, Y.Z. Yuan, Top. Catal. 57 (2014) 1015–1025.
[25] H. Adkins, H.R. Billica, J. Am. Chem. Soc. 70 (1948) 1095–1097.
[26] T.M. Ding, H.S. Tian, J.C. Liu, W.B. Wu, B.Q. Zhao, Catal. Commun. 74 (2016) 10–15.
[27] J.W. Zheng, H.Q. Lin, Y.N. Wang, X.L. Zheng, X.P. Duan, Y.Z. Yuan, J. Catal. 297 (2013) 110–118.
[28] J.F. Zhou, X.P. Duan, L.M. Ye, J.W. Zheng, M.M.J. Li, S.C.E. Tsang, Y.Z. Yuan, Appl. Catal. A Gen. 505 (2015) 344–353.
[29] G.S. Jeon, J.S. Chung, Korean J. Chem. Eng. 14 (1997) 49–58.
[30] P. Hirunsit, K. Faungnawakij, J. Phys. Chem. C 117 (2013) 23757–23765.
[31] L.L. Yu, J. Chen, J.W. Zheng, L.M. Ye, H.Q. Lin, Y.Z. Yuan, ChemCatChem 7 (2015) 1701–1707.
[32] Y.F. Zhu, Y.L. Zhu, G.Q. Ding, S.H. Zhu, H.Y. Zheng, Y.W. Li, Appl. Catal. A Gen. 468 (2013) 296–304.
[33] F. Frusteri, M. Cordaro, C. Cannilla, G. Bonura, Appl. Catal. B Envrion. 162 (2015) 57–65.
[34] Y.W. Lu, B.B. Cao, F. Yu, J. Liu, Z.H. Bao, J.S. Gao, ChemCatChem 6 (2014) 473–478.
[35] K. Xiao, X.Z. Qi, Z.H. Bao, X.X. Wang, L.S. Zhong, K.G. Fang, M.G. Lin, Y.H. Sun, Catal. Sci. Technol. 3 (2013) 1591–1602.
[36] T.M. Ding, H.S. Tian, J.C. Liu, W.B. Wu, J.T. Yu, Chin. J. Catal. 37 (2016) 484–493.